Designing Composite Triangular Subdivision Schemes

Peter Oswald

Bell Laboratories, Lucent Technologies
600 Mountain Avenue
Murray Hill, NJ 07974
e-mail: poswald@research.bell-labs.com

Abstract

Building subdivision schemes out of simple, very local and geometrically invariant averaging rules is convenient both from a theoretical and practical point of view. We review the benefits of this approach with special emphasis on the smoothness analysis of the limit surfaces, derive certain guidelines for how to design reasonable composite schemes, and apply those to hex-by-seven subdivision.

1 Introduction

Recently, there has been considerable interest in the classification of subdivision schemes, on the one hand, and in building a unified theory for the various existing variants of topology refinement and subdivision, on the other. A common theme in these investigations is that everything in subdivision is built upon a few primitives. E.g., the way the new mesh topology is defined through elementary polyhedral operators seems crucial, and suggests some very simple averaging operators and lower-order basic subdivision schemes (see [23, 27], [13, 15], [36]). A more general set of averaging rules for triangular meshes was considered in [31]. Data structures (mostly face-based and edge-based, see [3]) also influence what could be considered as the most basic schemes. The other common thread is the realization that repeating simple rules is a convenient way to create families of higher-order subdivision schemes.

Our angle here is to outline a design approach for families of composite triangular subdivision schemes that includes their smoothness analysis as an integral part. It summarizes the observations made in [31, 21], where specifically $\sqrt{3}-$subdivision schemes have been treated. The approach also covers hexagonal subdivision which is the face-based counterpart of vertex-based triangular subdivision. We apply it to $\sqrt{7}$-subdivision schemes which in their hexagonal interpretation have appeared in connection with pyramid schemes for modeling the function of the retina [37, 26] resp. for representing terrain data in geophysical applications [35].

The exposition is simplified by imposing some restrictions. We consider only triangular topologies without boundary, and assume that in the topology refinement step the

old vertex set is a subset of the new one. The latter assumption excludes some of the dual and mixed schemes discussed in [13] and also many of the meta-schemes proposed in [23, 27] but still includes the most common primal and dual subdivision schemes on triangular meshes with different dilation factors. We do not discuss quadrilateral and mixed topologies (say, mixtures of quads and triangles that will not disappear given certain topology refinement rules, see, e.g., [24, 28]), boundary treatment, adaptivity, etc.. The material is grouped into 3 sections. In Section 2 we introduce basic terminology. The guidelines for constructing higher-order composite schemes are collected and motivated by the resulting simplifications in the analysis in Section 3. In the final Section 4 the design rules are applied to construct $\sqrt{7}$- resp. hex-by-seven subdivision schemes.

2 Terminology

We will introduce subdivision schemes by separately describing the topology refinement rules (connectivity of the triangular mesh) and the geometry refinement (local averaging rules to position the geometric elements in $\mathbb{R}^3$).

In its face-based representation, a *triangular mesh topology* $\mathcal{T} := (\mathcal{V}, \mathcal{F})$ is given by a vertex set $\mathcal{V}$ (normally a list of integers) and a face set $\mathcal{F} \subset \mathcal{V} \times \mathcal{V} \times \mathcal{V}$. If $f = (v_1, v_2, v_3) \in \mathcal{F}$ then the 3 vertices v_i must be pairwise different, and are called the vertices of f (for short, $v_i \subset f$). Similarly, $e_1 = (v_1, v_2)$, $e_2 = (v_2, v_3)$, $e_3 = (v_3, v_1)$ are called the edges of f ($e_i \subset f$), and we will denote the set of all such edges by $\mathcal{E} \subset \mathcal{V} \times \mathcal{V}$. For the moment being edges are considered to have no orientation, and we will identify the edges (v, v') and (v', v). Similarly, two faces are the same if their vertex sets are identical (the order of the vertex triple does not matter). The basic compatibility condition (which also implies that there is no boundary) is that for any face f and any of its edges $e \subset f$, there is exactly one face $f' \neq f$ such that $e \subset f'$ (we call e the common edge of f and f'). Finally, we assume that the valence $k := k(v)$, i.e., the number of different faces f attached to a vertex v ($v \subset f$), is always finite but at least 3. Thus, each vertex $v \in \mathcal{V}$ has a natural *vertex* or 1-*ring neighborhood* $N(v)$ containing k vertices v_i, k faces $f_i = (v, v_i, v_{i+1})$, and k edges $e_i = (v, v_i) = f_i \cap f_{i-1}$ ($v_{k+1} = v_1$, $f_0 = f_k$) attached to it. Similarly, each face $f \in \mathcal{F}$ has a natural *face* or *flap neighborhood* $N(f)$ containing 3 more faces f_i besides f, and 3 vertices v_i and edges e_i directly attached to it. There is also a basic *edge neighborhood* $N(e)$ consisting of the two faces f_1 and f_2 that share this edge, its two endpoint vertices v_i, and 4 more edges e_i. These neighborhoods are easily accessible through the basic geometric data structures. Figure 1 illustrates them. Note finally that, instead of choosing $\mathcal{V}, \mathcal{F}$ as the primary entities and deriving the edge set $\mathcal{E}$ from them, we could also declare $\mathcal{V}$, $\mathcal{E}$ as primary, and define the face set $\mathcal{F}$ from them. This is related to edge-based data structures (see [3] for some motivation) but will not be pursued here.

General *polygonal mesh topologies* are defined in the same way, with the exception that faces are defined as $n(f)$-tuples, i.e., have $n(f)$ edges and vertices, where $n(f) \geq 3$ is finite and may change from face to face. As a consequence, the above described neighborhoods may become much more complicated. An example is the dual $\mathcal{T}^* = (\mathcal{V}^*, \mathcal{F}^*)$ of a triangular mesh topology $\mathcal{T}$ which is obtained by identifying $\mathcal{V}^* := \mathcal{F}$ and

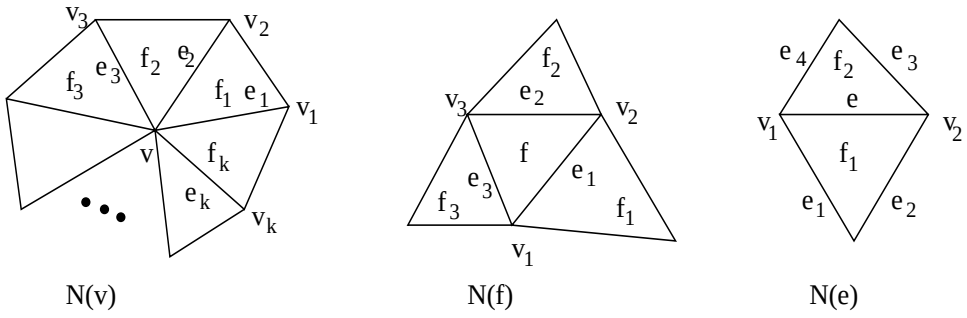


Figure 1: Basic vertex, face, and edge neighborhoods in triangular mesh topologies

$\mathcal{F}^* \cong \mathcal{V}$ in the sense that the face f^* associated with $v \in \mathcal{V}$ is given by the $k(v)$-tuple $(v_1^*, \ldots, v_{k(v)}^*) \equiv (f_1, \ldots, f_{k(v)})$. Since $n(f) \equiv 3$ for the original triangular mesh topology $\mathcal{T}$, we have $k(v^*) \equiv 3$ for all $v^* \in \mathcal{V}^*$ while $n(f^*) = k(v)$ becomes variable. Figure 2 shows portions of $\mathcal{T}$ and its dual $\mathcal{T}^*$. Since often the majority of vertices in a triangular topology has valence 6, the dual $\mathcal{T}^*$ is also referred to as *hexagonal mesh topology*.

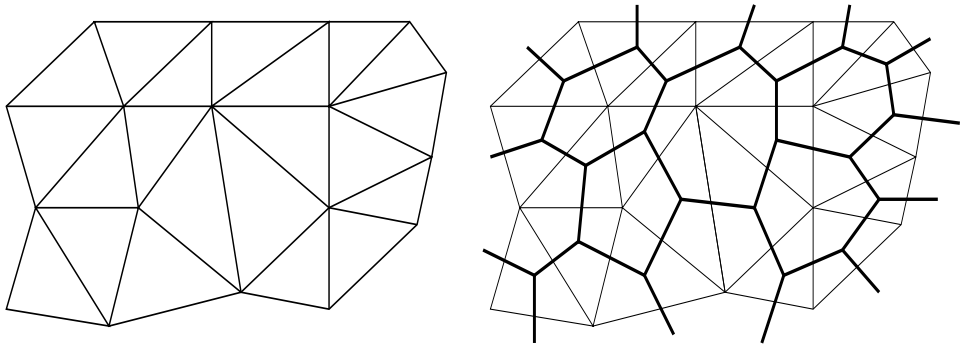


Figure 2: a) Triangular $\mathcal{T}$ and b) its dual $\mathcal{T}^*$ (or hexagonal) mesh topologies

The *topology refinement* is a procedure

$$TR \; : \qquad \mathcal{T} = (\mathcal{V}, \mathcal{F}) \quad \longmapsto \quad \mathcal{T}' = (\mathcal{V}', \mathcal{F}'),$$

applicable to an arbitrary triangular mesh topology $\mathcal{T}$. Usually, it is cast in geometric terms like vertex-, face-, or edge-splitting (see [38] for an example), and can be explained best on triangulations embedded into $\mathbb{R}^2$. A more systematic approach applicable to general mesh topologies is the representation of TR as a composition of a few elementary polyhedra operators [15] which is very close in spirit to our approach. Since we do not aim at utmost generality, we will just describe the assumptions on TR followed in this paper. First of all, we will always assume $\mathcal{V} \subset \mathcal{V}'$, and postulate that TR is *uniform* and *local*. This vaguely means that new $\mathcal{T}'$ is created by inserting a constant number of new vertices into each old triangle of $\mathcal{T}$ and connecting them following the same procedure everywhere. In particular, the application of TR to a uniform 3-directional triangular mesh of $\mathbb{R}^2$ must lead to another, down-scaled by a factor $\sqrt{m}$, and possibly rotated uniform 3-directional triangular mesh, where $m > 1$ is an integer (called *dilation*

factor). We will not further formalize these assumptions as they are usually clear from the context. Figure 3 a) shows the example of $\sqrt{3}$-refinement, where the geometric rule

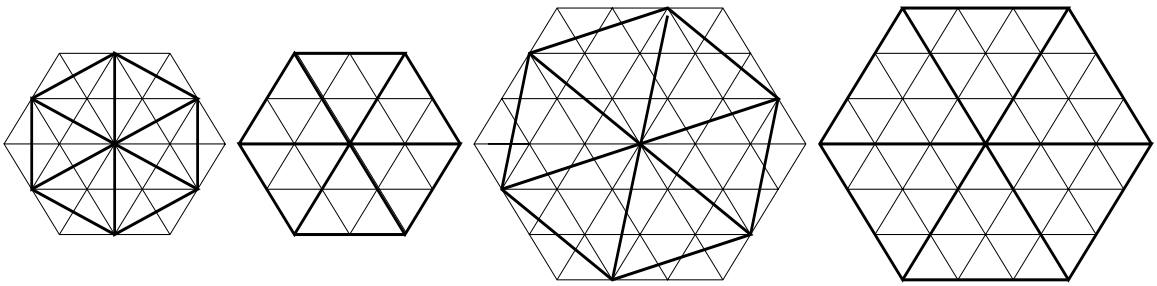


Figure 3: The triangular TR with $m \leq 9$ in the uniform setting

underlying TR is barycenter insertion (i.e,. one new vertex per face), and creating $\mathcal{F}'$ as the set of all triangles with one old vertex v and two new vertices v_1, v_2 such that the latter are the barycenters of two faces sharing a common edge with endpoint v. Following [26] or [13], it is easy to find all theoretically possible scaling factors $\sqrt{m}$ under these assumptions, they are given by the formula

$$m = k^2 - kl + l^2, \qquad l = 0, 1, \ldots, [k/2], \quad k \geq 2,$$

and can be found from the fact that all possible embeddings of a uniform 3-directional triangular mesh into another one are (up to symmetry and shift transformations) described by an edge of length $\sqrt{m}$ connecting two vertices of the finer triangulation. Figure 3 b)-d) shows these embeddings for some more values of m. Note that for $m \leq 48$ and up to symmetry transformations, the uniform TR for triangular mesh topologies with $\mathcal{V} \subset \mathcal{V}'$ are uniquely determined by the dilation factor m, however, one has to be careful with choosing the representer TR consistently, to use the analysis tools explained in Section 3 correctly (we come back to this in Section 4).

Only values $m \leq 9$ are probably of practical interest since the storage associated with $\mathcal{T}$ grows as $\sim m^j$ with the number of refinement steps j. However, if subdivision is performed as part of an adaptive pyramid transform, larger values of m might provide fast zoom-in features, see [26] for an example with $m = 19$. Our assumptions exclude values such as $m = 2$ (quincunx schemes) or $m = 5$ which can only be realized in quadrilateral mesh topologies resp. in schemes where the condition $\mathcal{V} \subset \mathcal{V}'$ is relaxed (see [7] for an example).

The description of the mesh topology is complemented by an embedding of $\mathcal{T}$ into $\mathbb{R}^3$ (or $\mathbb{R}^n$ for that matter) which allows us to interpret the mesh as a discrete surface in space. Generally, the embedding σ can be *vertex-based* $\sigma_{\mathcal{V}} : \mathcal{V} \longmapsto \mathbb{R}^3$, *face-based* $\sigma_{\mathcal{F}}$ $\mathcal{F} \longmapsto \mathbb{R}^3$, *edge-based* $\sigma_{\mathcal{E}} : \mathcal{E} \longmapsto \mathbb{R}^3$, or *mixed*, i.e., a collection of several such mappings. E.g., the point set $\sigma_{\mathcal{V}}(\mathcal{V})$ yields a triangulated surface in $\mathbb{R}^3$ after local linear interpolation w.r.t. each triangle of $\mathcal{F}$ is performed. Triangulated surfaces can be associated with $\sigma_{\mathcal{F}}$ and $\sigma_{\mathcal{E}}$ in various ways, too, but we will not dwell on these

details. Similarly, the topology refinement TR needs to be complemented by a *geometry refinement operator* GR which describes the way the embedding for the refined mesh topology $\mathcal{T}'$ is obtained from the one for $\mathcal{T}$. The most popular cases are *vertex-based* GR mapping $\sigma_{\mathcal{V}}$ into $\sigma_{\mathcal{V}'}$ (often called *primal subdivision schemes*), and *face-based* GR mapping $\sigma_{\mathcal{F}}$ into $\sigma_{\mathcal{F}'}$ (also called *dual subdivision schemes*). This terminology is natural since a face(vertex)-based GR on $\mathcal{T}$ can be interpreted as vertex(face)-based GR on the dual $\mathcal{T}^*$ vice versa. In particular, any vertex-based subdivision scheme for hexagonal mesh topologies is equivalent to a face-based subdivision scheme on the dual triangular mesh topologies, and there is no need to do a separate analysis for hexagonal meshes if face- and vertex-based schemes are studied in the triangular case. Edge-based GR have not been studied explicitly in connection with geometric modeling although they come up implicitly in the form of prolongation operators for multigrid solvers for certain elliptic systems of PDE such as Stokes or Maxwell equations.

Typically, a GR is given by *coefficient stencils*. E.g., for a vertex-based scheme, the stencil associates with each $v' \in \mathcal{V}'$ a geometrically invariant neighborhood $N_{GR}(v') \subset \mathcal{V}$ and weight function $w: N_{GR}(v') \to \mathbb{R}$, and defines the linear GR operation as follows:

$$\sigma_{\mathcal{V}'}(v') = \sum_{v \in N_{GR}(v')} w(v)\sigma_{\mathcal{V}}(v), \qquad 1 = \sum_{v \in N_{GR}(v')} w(v). \tag{1}$$

The neighborhood must not depend on the location of v' in $\mathcal{V}'$ but only on the type of v' which is determined by the corresponding TR. The weight normalization condition stated in (1) will always be assumed.

Finding appropriate stencils becomes cumbersome for larger m and higher-order schemes. For regular mesh topologies, we refer to [10]. An alternative [31] is to construct stencils by composing a few basic operations: A simple stencil for GR followed (and possibly preceded) by averaging rules that are applicable not only on regular mesh topologies. A *triangular averaging rule* AR is similar to a GR, with the only difference that it transforms an embedding σ associated with $\mathcal{T}$ into a new one for the same $\mathcal{T}$. For simplicity, only AR which map σ_X into σ_Y are considered, where X, Y are place-holders for $\mathcal{V}, \mathcal{F}, \mathcal{E}$, respectively. They can be described again by coefficient stencils, i.e., by geometrically invariant neighborhoods of vertices, faces, edges associated with $\mathcal{T}$ (not with $\mathcal{T}'$) as shown in Fig. 1 and weight functions on them. To have enough flexibility, we fix a *basic* AR for each X, Y combination, and denote it for our convenience by $Y \overset{c}{\leftarrow} X$, where the parameter c is present only if $X = Y$. This gives the 9 stencils depicted in Fig. 4, where $k = k(v)$ denotes the valence of the center vertex v.

Since the AR only act on one and the same triangular mesh topology $\mathcal{T}$, we need at least one GR that transfers information on $\mathcal{T}$ to information on the refined mesh topology $\mathcal{T}'$. According to our assumptions, there is one GR called *trivial upsampling* which does not depend on the geometric details of the particular TR:

$$GR_m: \qquad \sigma_{\mathcal{V}} \longmapsto \sigma_{\mathcal{V}'}(v') = \begin{cases} m\sigma_{\mathcal{V}}(v'), & v' \in \mathcal{V}, \\ 0, & v' \in \mathcal{V}' \backslash \mathcal{V}. \end{cases} \tag{2}$$

Using GR_m will lead to simplifications in the smoothness analysis.

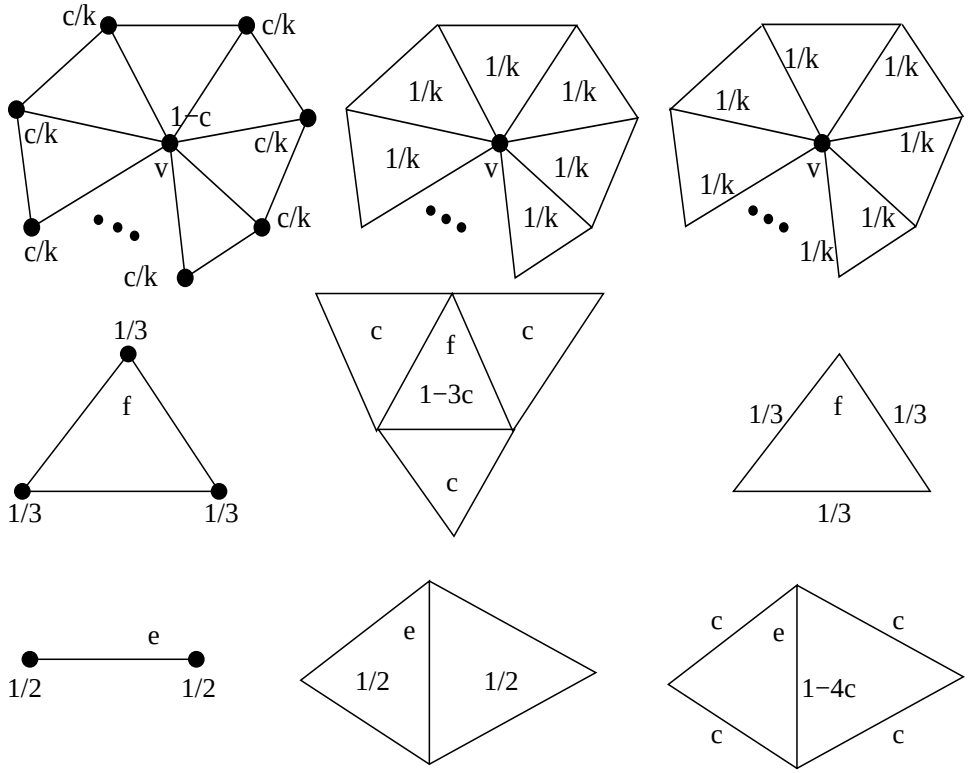


Figure 4: The 9 basic AR for obtaining v-values (top row), f-values (center row) resp. e-values (bottom row)

With all this terminology at hand, let us define a *composite subdivision operator* S on triangular mesh topologies and for a TR with dilation factor m by

$$S := AR'_{N_2} \circ \ldots \circ AR'_1 \circ GR_m \circ AR_{N_1} \circ \ldots \circ AR_1, \tag{3}$$

where $\{AR_n = X_n \overset{(c)}{\leftarrow} X_{n-1}\}$ is a collection of $N_1 \geq 0$ averaging rules acting on $\mathcal{T}$ such that $X_{N_1} = \mathcal{V}$, and $\{AR'_n = Y_n \overset{(c)}{\leftarrow} Y_{n-1}\}$ is a collection of $N_2 \geq 0$ averaging rules acting on $\mathcal{T}'$ such that $Y_0 = \mathcal{V}'$. Clearly, to be compatible with our above restrictions on the GR to be considered, we also assume that $Y_{N_2} = X'_0 := X'$. Finally, the *subdivision scheme* associated with S consists of applying S iteratively, starting from an initial triangular mesh topology $\mathcal{T}^0$ and embedding $\sigma^0 := \sigma_{X^0}$. This creates a sequence $\{(\mathcal{T}^j, \sigma^j)\}$, $j \geq 0$, where $\mathcal{T}^{j+1} = (\mathcal{T}^j)'$ is the result of applying TR, and $\sigma^{j+1} = S\sigma^j$. Since we apply the same TR and S for each j, the scheme is called *stationary*. The goal of the analysis of any such scheme is to make sure that the point sets given by σ^j (more precisely: the associated triangulated surfaces) converge to a limit surface $S^\infty\sigma^0$ of reasonable shape and smoothness properties for generic initial configurations $(\mathcal{T}^0, \sigma^0)$. In this analysis, the composition structure of S can advantageously be explored, as will be explained in the next section. Examples of primal/dual composite triangular subdivision schemes for $m = 3, 4$ can be found in [31, 8].

3 Smoothness Analysis and Design of Composite Schemes

3.1 Generalities on Convergence and Smoothness

The smoothness analysis of stationary subdivision schemes is usually separated into two steps, the analysis in the regular case (a mesh topology that is embedded into a 3-directional uniform mesh of $\mathbb{R}^2$) and a certain number of singular cases (here, the situation near extraordinary vertices of valence $k \neq 6$). It is based on viewing the limit surface (and all intermediate triangulated surfaces associated with σ^j) as covered by local charts, i.e., parametric mappings from $\mathbb{R}^2$ into $\mathbb{R}^3$, whose domains Ω_ν correspond to overlapping triangular patches F_ν in some fixed $\mathcal{T}^{j_0}$. E.g., one could consider one chart per 1-ring neighborhood of faces $N(v)$ for each $v \in \mathcal{T}^{j_0}$. Because of finite stencil support, for $j \geq j_0$ the local charts will depend only on the restriction of $(\mathcal{T}^{j_0}, \sigma^{j_0})$ to some small neighborhood $\tilde{F}_\nu$ of F_ν. Thus, by embedding these extended triangular patches $\tilde{F}_\nu \supset F_\nu$ suitably into the plane (this results in domains $\tilde{\Omega}_\nu \supset \Omega_\nu$), we can study convergence and smoothness locally by looking at the subdivision process on each $\tilde{F}_\nu$. Moreover, this can be done in a functional setting (by looking at functions from $\tilde{\Omega}_\nu \supset \Omega_\nu$ into $\mathbb{R}$ rather than into $\mathbb{R}^3$).

Simplifications come from the fact that by using the uniformity of TR and taking j_0 large enough, the patches $\tilde{F}_\nu \supset F_\nu$ and their embeddings in the plane $\tilde{\Omega}_\nu \supset \Omega_\nu$ can be chosen such that only a few different types of $\tilde{\Omega}_\nu$ occur, and that those can be viewed as part of some generic triangulations of $\mathbb{R}^2$. In other words, by using appropriate local charts as vehicle, we are able to switch from the investigation of subdivision schemes for parametric surfaces associated with arbitrary triangular mesh topologies to the investigation of subdivision schemes for scalar functions over a few special triangulations on $\mathbb{R}^2$. For triangular mesh topologies, only two such special triangulations are required, *a uniform type-I triangulation of* $\mathbb{R}^2$ and a *valence-k rotationally-invariant triangulation.* A type-I triangulation is shown in Fig. 5 b), and a valence-4 rotationally-invariant triangulation in Fig. 5 c), together with sample regions $\tilde{\Omega}_\nu \supset \Omega_\nu$ as they would look for Loop's scheme [25]. Fig. 5 a) shows a planar version of the original $\mathcal{T}^{j_0}$ with $j_0 = 2$, it is easy to see that any $\mathcal{T}^2$ can be covered by families of sets $F_\nu \subset \tilde{F}_\nu$ with enough overlap, and with regions $\tilde{\Omega}_\nu$ corresponding to either Fig. 5 b) or c).

The investigation of subdivision schemes on uniform type-I triangulations is essentially equivalent to the theory of *refinable vectors.* Reviews of the latter with emphasis on applications to subdivision can be found in [4, 17, 21, 10, 6]. Here is a summary of the necessary ingredients:

- The *dimension of the refinable vector* is $r = 1$ for vertex-based, $r = 2$ for face-based, and $r = 3$ for edge-based schemes. The components of the vectors are associated with the 2 types of faces resp. 3 types of edges in a type-I triangulation.

- The *dilation matrix* M is an integer 2×2 matrix M with $\det(M) = m$ and isotropic spectrum ($|\lambda_1| = |\lambda_2| = \sqrt{m}$) which is determined by the associated TR. There are usually several possible M, and one has to fix one by assuring that M maps

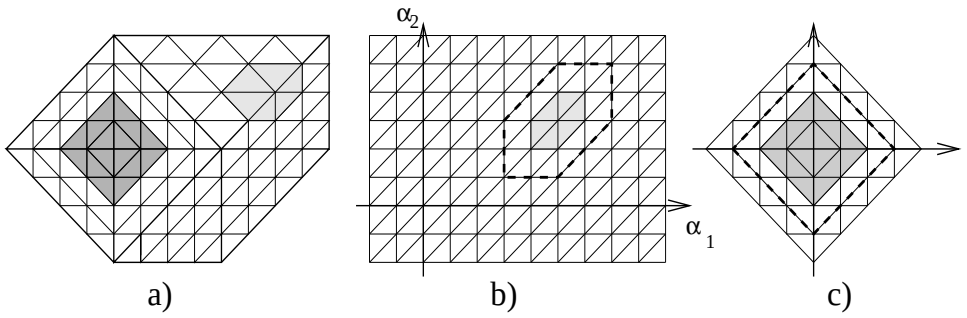


Figure 5: Examples of local patches F_μ, and their embedding into standard triangulations (F_ν and Ω_ν are shaded, the dashed lines indicates the boundary of $\tilde{\Omega}_\nu$)

$\mathbb{Z}^2 = \mathcal{V}'$ onto the set $\mathcal{V}$ of old vertices $v \in \mathcal{V}$. The identification of $\mathbb{Z}^2$ with $\mathcal{V}'$ is in agreement with Fig. 6 b), and induces (through the application of M) an identification of $\mathcal{V}$ with $\mathbb{Z}^2$. E.g., with the plots in Fig. 3 properly transformed to a square lattice as shown in Fig 6 b), we get

$$M_3 = \begin{pmatrix} 2 & -1 \\ 1 & 1 \end{pmatrix}, \quad M_4 = \begin{pmatrix} 2 & 0 \\ 0 & 2 \end{pmatrix}, \quad M_7 = \begin{pmatrix} 3 & -1 \\ 1 & 2 \end{pmatrix}, \quad M_9 = \begin{pmatrix} 3 & 0 \\ 0 & 3 \end{pmatrix},$$

for $\sqrt{3}-$, $2-$, $\sqrt{7}-$, and $3-$refinement. The identification of $\mathcal{V}$, $\mathcal{V}'$ allows us from now on to replace functions such as $\sigma_\mathcal{V}$ by $\mathbb{Z}_2$ sequences, similarly, $\sigma_\mathcal{F}$ and $\sigma_\mathcal{E}$ can be represented by $\mathbb{Z}_2$ sequences of vectors with r components.

- The *mask* $P := \{P_\alpha,\ \alpha \in \mathbb{Z}^2\}$ is a finitely supported sequence of $r \times r$ matrices describing the stencil information for S. Their definition from S is simple: In the vertex-based case, the P_α are scalars and found as the values on $\mathbb{Z}^2$ after one subdivision step if the sequence $\sigma_\mathcal{V}$ is set to 1 at the origin, and 0 at all other $0 \neq \alpha \in \mathbb{Z}^2$, i.e., if $\sigma_\mathcal{V} = \delta_0$. Since $\mathcal{V}$ is $M\mathbb{Z}^2$-shift-invariant by definition of S the result of S applied to $\sigma_\mathcal{V} = \delta_\beta$ would be the same sequence but shifted by $-M\beta$. Thus, we easily obtain

$$\sigma_{\mathcal{V}'}(\alpha) = \sum_{\beta \in \mathbf{Z}^2} P_{\alpha - M\beta} \sigma_\mathcal{V}(\beta). \tag{4}$$

  An analogous formula holds for the face- and edge-based case, with the only difference that (4) has to be understood in vector-matrix notation. In summary, in the regular case, subdivision schemes can be studied as iterations of convolution type operators acting on vector $\mathbb{Z}^2$ sequences.

- To understand the convergence and smoothness properties of the scheme, we need to study the solutions $\Phi : \mathbb{R}^2 \to \mathbb{R}^r$ of the associated *refinement equation*,

$$\Phi = \sum_{\alpha \in \mathbf{Z}^2} P_\alpha \Phi(M \cdot - \alpha). \tag{5}$$

  and the *cascade iteration*

$$\Phi^{j+1} = \sum_{\alpha \in \mathbf{Z}^2} P_\alpha \Phi^j(M \cdot - \alpha), \qquad j \geq 0, \tag{6}$$

where $\Phi^0 : \mathbb{R}^2 \to \mathbb{R}^r$ is a compactly supported vector function. It is easy to see that if the cascade iteration produces a L_p convergent sequence Φ^j then its limit is a compactly supported L_p solution to (5).

The connection to subdivision is straightforward: If Φ^0 is chosen appropriately, then

$$g^j := \sum_{\alpha \in \mathbf{Z}^2} \sigma^j(\alpha)^T \Phi^0(M^j \cdot - \alpha) = \sum_{\alpha \in \mathbf{Z}^2} \sigma^0(\alpha)^T \Phi^j(\cdot - \alpha), \qquad j \geq 0,$$

is related to the discrete surface given by σ^j. E.g., if we look at vertex-based schemes and take as Φ^0 the piecewise linear hat function positioned at the origin of a type-I triangulation (identified with $\mathcal{T}^0$ resp. $\mathbb{Z}^2$), then g^j coincides with the piecewise linear function associated with $(\mathcal{T}^j, \sigma^j)$. Thus, convergence of the cascade algorithm implies convergence of the subdivision scheme, and the limit $g = \lim_{j \to \infty} g^j$ is represented by a linear combination of the shifts $\Phi(\cdot - \alpha)$, and thus inherits its smoothness properties from Φ. With the proper choice of Φ^0, similar interpretations hold for face- and edge-based subdivision schemes.

- The investigation of (5) resp. (6) is essentially complete. E.g., the existence of a compactly supported distributional solution Φ of (5), the *order of polynomial reproduction* (or *sum rule order*) and local linear independence of the set of shifts $\{\Phi(\cdot - \alpha) : \alpha \in \mathbb{Z}^2\}$, can be decided in terms of algebraic condidtions on the mask P resp. its symbol

$$P(\omega) = m^{-1} \sum_{\alpha \in \mathbf{Z}^2} P_\alpha e^{-i\alpha\omega}, \quad \omega \in \mathbb{T}^2. \tag{7}$$

The convergence of the cascade iteration resp. smoothness of Φ as well as L_p-stability of the shifts $\{\Phi(\cdot - \alpha) : \alpha \in \mathbb{Z}^2\}$ need more elaborate tools. There are two basic approaches [17, 20, 18, 6], one is via Fourier transform techniques and uses the *transition operator*

$$(T_P X)(\omega) = \sum_{\tilde{\gamma} \in \tilde{\Gamma}} P(\omega_{\tilde{\gamma}}) X(\omega_{\tilde{\gamma}}) P(\omega_{\tilde{\gamma}})^* |_{\omega_{\tilde{\gamma}} = M^{-T}(\omega + 2\pi\tilde{\gamma})}, \quad \omega \in \mathbb{T}^2, \tag{8}$$

acting on non-negative definite Hermitean $r \times r$ matrix functions $X(\omega)$ but yields a complete theory only for L_2. The set $\tilde{\Gamma}$ is a fixed representer set for $\mathbb{Z}^2/(M^T\mathbb{Z}^2)$, and consists of m elements $\tilde{\gamma}$. The second approach uses the *ℓ_p-joint spectral radius* of the m operators

$$(A_\gamma \sigma)(\alpha) = \sum_{\beta \in \mathbf{Z}^2} P_{\gamma + M\alpha - \beta} \sigma(\beta) \tag{9}$$

with respect to a certain finite-dimensional subspace V_P determined by the mask P and its sum rule order. Here γ is chosen from a fixed representer set Γ of $\mathbb{Z}^2/(M\mathbb{Z}^2)$.

The latter approach is suitable for all L_p, $1 \leq p \leq \infty$, in particular, it covers the case of uniform convergence and Hölder smoothness ($p = \infty$). Its only drawback

is that the practical evaluation of joint spectral radii is computationally expensive, especially if m, r, or the mask support become larger while the assessment of L_2 smoothness properties via matrix transfer operators is less involved (it leads to a matrix eigenvalue problem whose dimension is linear in the number of non-zero mask coefficients P_α, and quadratic in r). Some software tools that support these tasks are described in [21, 10]. There is one partial case where the Hölder smoothness analysis is simplified: If $r = 1$ and the scalar symbol is non-negative, i.e., $P(\omega) \geq 0,\ \omega \in \mathbb{T}^2$, then the Hölder smoothness of Φ is determined by the spectral radius of one operator $A_0|_{V_P}$, and inexpensive to find.

After a scheme has been studied for type-I triangulations, it still needs to pass the test in the remaining irregular situations which in the case of triangulations is the behavior near *extraordinary vertices* represented by k-vertex rotationally invariant triangulations with $k \neq 6$. This theory has been developed mainly in [32, 28, 30, 40, 39], and requires the study of the characteristic map which goes beyond a simple eigenvalue analysis of the local subdivision operator associated with an appropriate invariant neighborhood of the origin in the k-vertex triangulation. To the best of our knowledge, a complete analysis of the characteristic map is still subject to a case-by-case approach, i.e., it has not been turned into a straightforward numerical procedure (see [39] for more information). As a compromise, often only a partial analysis is performed by verifying a necessary condition [32, 28, 40] for C^1 smoothness at the extraordinary vertex, namely, the existence of a pair of subdominant eigenvalues $\lambda_2 = \lambda_3^*$ ($\lambda_1 = 1 > |\lambda_2| = |\lambda_3| > |\lambda|_\mu$, $\mu \geq 4$) associated with specific eigenvectors in the discrete Fourier basis of the local subdivision operator, and by checking the soundness of the characteristic map visually. For a simplified analysis in the case of schemes with small stencils, see [14].

This approach seems to be acceptable in a design cycle, where one first wants to *find* a suitable method out of a variety of choices, but needs to be complemented by a more detailed analysis after a specific method has been selected. We mention that the problem of C^α smoothness with $\alpha > 1$ at extraordinary vertices, and of shape regularity of a subdivision surfaces in general is much more complex, and refer to [34, 2, 29] for recent discussions on this issue.

3.2 Simplifications for Composite Rules

Let us return to the class (3) of composite triangular subdivision operators. By rearranging the averaging rules, we will cast it in its canonical form as vertex-based scheme:

$$S_{\mathcal{V}} = A'_N \circ \ldots \circ A'_1 \circ GR_m, \qquad A'_n = \begin{cases} AR'_n, & n = 1, \ldots, N_1, \\ (AR_{n-N_1})', & n = N_1+1, \ldots, N = N_1 + N_2. \end{cases} \tag{10}$$

Here, $(AR_n)'$ denotes the averaging rule AR_n applied on $\mathcal{T}'$. It is crucial in the rearrangement step to maintain the order in which the averaging rules AR'_n and $(AR_n)'$ appear. In particular, this guarantees that all compositions $A'_{n+1} \circ A'_n$ make sense. It turns out (see [31] and below) that under mild conditions many properties of the original S in (3) can be deduced from properties of its associated $S_{\mathcal{V}}$, and that the investigation of the latter is simpler in many respects.

- We start with the regular case, i.e., we consider the subdivision operator (10) on a uniform type-I triangulation. Due to the transformation from S to $S_{\mathcal{V}}$, the associated refinement equation (5) will always be *scalar*. Having $r = 1$ will simplify the analysis.

- The symbol (7) will come in *factorized form*. Indeed, according to the definition of the mask coefficients P_α from the subdivision rule, it is obvious that the mask $P_{\mathcal{V}}$ of $S_{\mathcal{V}}$ is obtained by convoluting the masks P_n, $n = 1, \ldots, N$ (and multiplying the result by the factor m coming from GR_M). Note that the coefficients $(P_n)_\alpha$, $\alpha \in \mathbb{Z}^2$, of P_n can be found from the result of applying the averaging rule A'_n to the corresponding δ_0-sequence, and that

$$P_n(\omega) := \sum_{\alpha \in \mathbf{Z}^2} P_{n,\alpha} e^{-j\alpha\omega}$$

(there is no scaling by m^{-1} since this is the symbol for an averaging operator on the same mesh topology, and not of a subdivision operator). As a result,

$$P_{\mathcal{V}}(\omega) = P_N(\omega) \ldots P_1(\omega), \tag{11}$$

since the factor m from GR_m is cancelled by the normalization factor m^{-1} in the definition (7) applied to $P_{\mathcal{V}}(\omega)$. Due to the normalization condition for averaging rules, we always have $P_{\mathcal{V}}(0) = 1$. Note that though $P_{\mathcal{V}}(\omega)$ is scalar, among the $P_n(\omega)$ might be $r \times r'$ matrix symbols, with $r, r' = 1, 2, 3$ corresponding to the type of geometric entities involved in the definition of A'_n. For writing these symbols down, we identify vertices of the type-I triangulation with $\mathbb{Z}^2$ lattice points ($v_\alpha \equiv \alpha$), denote by e^1_α, e^2_α, e^3_α, the edges connecting α with $\alpha+(1,0)$, $\alpha+(0,1)$, $\alpha+(1,1)$, respectively, while f^1_α is the triangle with vertices α, $\alpha+(1,0)$, $\alpha+(1,1)$ and f^2_α the triangle with vertices α, $\alpha+(0,1)$, $\alpha+(1,1)$. Fig. 6 a) illustrates these conventions (for $\alpha = 0$, the subscript α is not shown). Then we can write down the symbols for the rules in Fig. 4. E.g., the 2×1 matrix symbol for $\mathcal{F} \leftarrow \mathcal{V}$ rules is

$$P_{\mathcal{F}\leftarrow\mathcal{V}}(\omega) = \begin{pmatrix} \frac{1}{3}(1 + e^{i\omega_1} + e^{i(\omega_1+\omega_2)}) \\ \frac{1}{3}(1 + e^{i\omega_2} + e^{i(\omega_1+\omega_2)}) \end{pmatrix},$$

the 2×2 matrix symbol for $\mathcal{F} \overset{c}{\leftarrow} \mathcal{F}$ is

$$P_{\mathcal{F}\overset{c}{\leftarrow}\mathcal{F}}(\omega) = \begin{pmatrix} 1 - 3c & c(1 + e^{-i\omega_1} + e^{i\omega_2}) \\ c(1 + e^{i\omega_1} + e^{-i\omega_2}) & 1 - 3c \end{pmatrix},$$

and 1×2 matrix symbol for $\mathcal{V} \leftarrow \mathcal{F}$ is

$$P_{\mathcal{V}\leftarrow\mathcal{F}}(\omega) = \frac{1}{6}\begin{pmatrix} 1 + e^{-i\omega_1} + e^{-i(\omega_1+\omega_2)} & 1 + e^{-i\omega_2} + e^{-i(\omega_1+\omega_2)} \end{pmatrix},$$

respectively. The mask coefficients can be read from Fig. 6 b)-d) where the action of the corresponding averaging rules on δ_0-sequences is displayed.

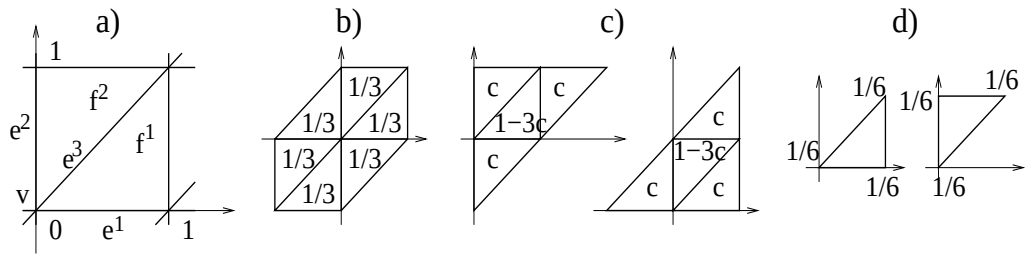


Figure 6: a) Notation for defining symbol entries ($\alpha = 0$), and results of applying b) $\mathcal{F} \leftarrow \mathcal{V}$, c) $\mathcal{F} \overset{c}{\leftarrow} \mathcal{F}$, resp. d) $\mathcal{V} \leftarrow \mathcal{F}$ to the corresponding δ_0-sequences

- The factorization can be used to verify *sum rule orders* which are related to the order of polynomial reproduction of the subdivision scheme. Loosely speaking, $S_\mathcal{V}$ has sum rule order $K \geq 1$ if it preserves polynomial sequences of degree $\leq K-1$ (at least, for the situation of uniform type-I triangulations). In particular, $S_\mathcal{V}$ has sum rule order 1 if it preserves constants, i.e., if $S_\mathcal{V}\{1\} = \{1\}$, which is easy to verify directly. Among the many equivalent definitions of sum rule orders, we mention the following algebraic condition in terms of the symbol: $S_\mathcal{V}$ has sum rule order K if $P_\mathcal{V}(0) = 1$ (this is always satisfied) and

$$\frac{\partial^\mu P_\mathcal{V}}{\partial \omega^\mu}(2\pi M^{-T}\tilde{\gamma}) = 0 \qquad \forall\, |\mu| < K \quad \forall\, 0 \neq \tilde{\gamma} \in \tilde{\Gamma}. \tag{12}$$

  Without loss of generality, we have assumed that $0 \in \tilde{\Gamma}$.

  Given two composite rules $S_\mathcal{V}^{(1)}$ and $S_\mathcal{V}^{(2)}$ for the same TR, we define their *concatenation* $(S^{(2)}S^{(1)})_\mathcal{V}$ as the composite scheme, where after GR_m first the averaging rules for $S_\mathcal{V}^{(1)}$ and then the averaging rules for $S_\mathcal{V}^{(2)}$ are performed in their respective orders.

  Lemma 1 *If $S_\mathcal{V}^{(1)}$, $S_\mathcal{V}^{(2)}$ are two subdivision operators given by (10), with sum rule orders K_1, K_2 (w.r.t. the same M), then their concatenations $(S^{(2)}S^{(1)})_\mathcal{V}$ and $(S^{(1)}S^{(2)})_\mathcal{V}$ coincide, and have at least sum rule order $K_1 + K_2$.*

  The elementary proof directly follows from (12) using the Leibniz rule for partial differentiation for the product $P_\mathcal{V}^{(2)}(\omega)P_\mathcal{V}^{(1)}(\omega) = P_\mathcal{V}^{(1)}(\omega)P_\mathcal{V}^{(2)}(\omega)$ which represents the symbol of the composite operators (scalar multiplication is commutative). A special corollary is as follows: *If the scheme $S_\mathcal{V}$ defined in (10) has sum rule order K, then $S_\mathcal{V}^L$ (the L-fold concatenation of $S_\mathcal{V}$) has sum rule order LK.* This allows us to obtain subdivision schemes with higher sum rule orders from schemes with $K = 1$ or $K = 2$ without difficulty which, in turn, is prerequisite for achieving schemes with very smooth limit surfaces.

- Since $r = 1$ and factorizations hold, simplifications in the *smoothness analysis* are possible. First of all, the formula for the transition operator simplifies to

$$(T_{P_\mathcal{V}}X)(\omega) = \sum_{\tilde{\gamma}\in\tilde{\Gamma}} |P_\mathcal{V}(\omega_{\tilde{\gamma}})|^2 X(\omega_{\tilde{\gamma}}), \qquad \omega_{\tilde{\gamma}} = M^{-T}(\omega + 2\pi\tilde{\gamma}), \quad \omega \in \mathbb{T}^2, \tag{13}$$

and solely depends on the squared symbol $|P_{\mathcal{V}}(\omega)|^2 \geq 0$, and the L_2-smoothness issue is completely covered in [11, 19], where also references to previous work can be found. Software for computing the best possible values of the Sobolev smoothness exponent of the associated refinable function $\Phi_{\mathcal{V}}$ based on these papers (and the later [20, 18] for the vector case) is available from the webpages of the authors of [21], [9, 10], [33].

Concerning the estimation of the *Hölder smoothness exponent*

$$s_\infty(\Phi) = \inf\{s \geq 0 : \ \Phi_l \in C^s(\mathbb{R}^2), \ l = 1, \ldots, r\}.$$

of $\Phi = (\Phi_1, \ldots, \Phi_r)^T$, there are 3 basic approaches. First of all, the trivial lower bound

$$s_\infty(\Phi) \geq s_2(\Phi) - 1$$

follows from the embedding $H^{s+1+\epsilon}(\mathbb{R}^2) \subset C^s(\mathbb{R}^2)$, $s \geq 0$, $\epsilon > 0$, and relates the Hölder exponent to the L_2-Sobolev exponent $s_2(\Phi)$ which is easier to obtain ([10, 12] promote this approach).

Secondly, for concatenated schemes one can use convolution arguments: If the refinable functions $\Phi_{\mathcal{V}}^{(i)}$ corresponding to the subdivision operators $S_{\mathcal{V}}^{(i)}$ have Hölder exponents $s_\infty(\Phi_{\mathcal{V}}^{(i)}) > 0$, $i = 1, 2$, then the refinable function associated with the concatenated scheme $(S^{(1)}S^{(2)})_{\mathcal{V}} = (S^{(2)}S^{(1)})_{\mathcal{V}}$ is given by convolution $\Phi = \Phi_{\mathcal{V}}^{(1)} * \Phi_{\mathcal{V}}^{(2)}$, and thus satisfies

$$s_\infty(\Phi) \geq s_\infty(\Phi_{\mathcal{V}}^{(1)}) + s_\infty(\Phi_{\mathcal{V}}^{(2)}).$$

Although this inequality is not necessarily sharp, it allows us to reduce the consideration for complicated concatenated schemes to estimates for Hölder smoothness exponents of their components which might be easier to obtain. In particular, for the refinable function $\Phi_{\mathcal{V}}^L$ associated with the L-fold concatenation $S_{\mathcal{V}}^L$ of $S_{\mathcal{V}}$, this approach gives the lower bound $s_\infty(\Phi_{\mathcal{V}}^L) \geq L s_\infty(\Phi_{\mathcal{V}})$, i.e., guarantees linear growth of the Hölder smoothness for $L \to \infty$, if $s_\infty(\Phi_{\mathcal{V}}) > 0$. This fact has been explored in [8].

Finally, we can use the joint spectral radius criterion [11, 18] which gives the precise geometric decay of the K-th order differences of the subdivision sequences σ^j (that estimating this decay is crucial for proving Hölder continuity of limit surfaces in subdivision processes is well-known, and has been used in many papers, see [4, 6]). Since computable lower and upper bounds for the joint spectral radius converge very slowly to the exact value while requiring large computational resources, it is very desirable to use shortcuts whenever possible. We mention one partial case of composite schemes where the Hölder exponent can be computed in an efficient way: If L is *even* and the symbol $P_{\mathcal{V}}(\omega)$ of a composite scheme $S_{\mathcal{V}}$ is real-valued, then the concatenated scheme $S_{\mathcal{V}}^L$ has obviously a non-negative symbol $P_{\mathcal{V}}(\omega)^L \geq 0$. Consequently, $s_\infty(\Phi_{\mathcal{V}}^L)$ is computable as the spectral radius of a single matrix, see e.g. [16].

- What concerns the quality of composite triangular subdivision schemes near extraordinary vertices with valence $k \neq 6$, some interesting observations have been made in [31]. It turns out that normally the C^1 property holds for all valences, with the exception of $k = 3$. To overcome the problems for $k = 3$, and to obtain visually pleasing surfaces after a few subdivision steps, some modifications of the basic AR have been proposed in [31]. E.g., if the basic rule $\mathcal{F} \leftarrow \mathcal{V}$ is among the averaging rules then it can be modified as shown in Fig. 7 a), where a special weight factor $w = w(k)$ is introduced if one of the vertices of the triangle has valence $k \neq 6$. Note that triangles with more than one extraordinary vertex can appear only in the first subdivision step. It has been observed that often a slight increase $w > 0$ is sufficient for proving the C^1 property at vertices of valence $k = 3$, and that choices $w(k) > 0$ for $k < 6$ and $w(k) < 0$ for $k > 6$ improve the fairness of the discrete surfaces. Almost any of the basic AR in Figure 4 could potentially be modified near extraordinary vertices. Fig. 7 b) and c) show such modifications for $\mathcal{F} \overset{c}{\leftarrow} \mathcal{F}$ resp. for $\mathcal{V} \leftarrow \mathcal{F}$ (in [31], the latter was called flap modification).

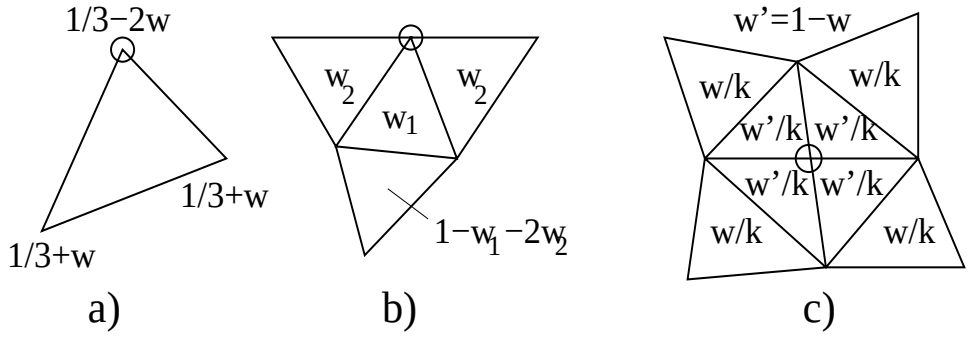


Figure 7: Weight modifications for a) $\mathcal{F} \leftarrow \mathcal{V}$, b) $\mathcal{F} \overset{c}{\leftarrow} \mathcal{F}$, and c) $\mathcal{V} \leftarrow \mathcal{F}$

Unfortunately, in contrast to the regular case, there are currently no simplifying statements that apply to the smoothness analysis of composite schemes near extraordinary vertices. E.g., concatenation of "good" rules may not necessarily result in a good scheme. The only general result for composite schemes, which holds both in the regular and irregular cases, is about the connection of the smoothness properties of the general composite subdivision operator S given by (3) and its vertex-based rearrangement $S_{\mathcal{V}}$ given by (10). It turns out that under mild assumptions on (3) the properties of S cannot be worse than those of $S_{\mathcal{V}}$. More precisely, we have the following

Lemma 2 *Let S and $S_{\mathcal{V}}$ be defined by (3) and (10), respectively, and assume that the part*

$$S' := AR'_{N_2} \circ \ldots \circ AR'_1 \circ GR_m$$

of S preserves constant sequences. Then the subdivision scheme S converges for generic bounded initial data to a $C^{\alpha}_{\mathrm{loc}}$ limit surface if $S_{\mathcal{V}}$ does so. More precisely, if ϕ_v is the limit of recursively applying $S_{\mathcal{V}}$ to the delta-sequence δ_v associated with

a vertex $v \in \mathcal{V}^0$ then the limit ϕ_x under the recursive application of S to a delta-sequence δ_x associated with a geometric entity x from X^0 can be represented as a linear combination of the former (the coefficients of which are determined by the composite averaging rule $AR_{N_1} \circ \ldots \circ AR_1$).

The proof of this result is essentially the same as the one given in [31] for the particular case $AR_1 = \mathcal{V} \leftarrow \mathcal{F}$ ($N_1 = 1$), and will not be reproduced here.

3.3 Design Rules

From the above, we summarize the following approach to designing composite schemes covering both the triangular and, via duality, hexagonal mesh case.

A Determine the type of topological refinement, and dilation factor m. On a regular type-I triangulation, fix the corresponding dilation matrix M.

B By using the trivial subdivision operator GR_m and a few basic averaging rules $A_i = X_i \leftarrow X_{i-1}$, where $i = 1, \ldots, N$ and $X_0 = X_N = \mathcal{V}$, compose a vertex-based subdivision operator $S_\mathcal{V}$ as in (10) such that it reproduces at least constant sequences, preferably, linear sequence functions, i.e., possesses sum rule order $K = 1$ or $K = 2$. The verification for $K = 2$ may be confined to the situation of a regular type-I triangulation. If the interest is in primal hexagonal schemes (or dual triangular schemes), make sure that among the X_i with $i = 1, \ldots, N-1$ there is at least one $\mathcal{F}$. This whole task depends on the topological refinement rule, and requires some qualified guesses. However, it is usually not difficult to come up with one or several such lower-order composite rules by using as few as possible AR_i.

C Suppose that in Step B a candidate $S_\mathcal{V}$ has been found. Then consider the family $S_\mathcal{V}^L$, $L \geq 1$, and check its properties in the regular case using the theory of refinable functions. For small L this can usually be done with the software tools developed in [21, 9, 12], while for large L good lower smoothness estimates follow from the outlined convolution argument. It is also recommended to investigate the stability of the set of shifts $\{\Phi(\cdot - \alpha),\ \alpha \in \mathbb{Z}^2\}$ and the Sobolev regularity, as this might be of interest for applications of the subdivision approach in simulations. If m or the complexity of $S_\mathcal{V}$ are increasing, the exact computation of Hölder exponents might become impractical, and one might restrict the attention to even L, where $P_\mathcal{V}(\omega)^L \geq 0$. Finally, if several candidate $S_\mathcal{V}$ are available then other suitable concatenations besides $S_\mathcal{V}^L$ may be tried.

D Among the cases investigated in the last step, choose a scheme which has Hölder smoothness $s_\infty > 2$, i.e., is at least C^2 on regular grids, and investigate the associated local subdivision operator for a $k(\neq 6)$-vertex rotationally invariant triangulation. This investigation involves some modification of one or several of the A_i near the extraordinary vertex, as suggested in the previous subsection. To achieve the C^1-property globally, such modifications are necessary only for low-valence cases such as $k = 3$ but may be useful for surface fairing as well.

E Under the assumptions of Lemma 2, the results of the analysis of $S_{\mathcal{V}}$ automatically hold for those vertex- (primal), face- (dual), and edge-based composite schemes S of the form (3) which are given by proper rearrangements of the components of $S_{\mathcal{V}}$ as discussed above. In particular, if S with $X_0 = Y_{N_2} = \mathcal{F}$ are among the admissible rearrangements of $S_{\mathcal{V}}$, then we arrive at hexagonal schemes. This makes a separate analysis for the hexagonal case unnecessary.

4 $\sqrt{7}$-Triangular and Hex-by-7 Subdivision Schemes

In this concluding section, we will follow the above design approach for $\sqrt{7}$ resp. hex-by-7 subdivision. It seems that until now there is no general proposal for $m = 7$, which makes this a non-trivial test case. Note that the more popular cases $m = 3$ ($\sqrt{3}$-subdivision [22, 31, 21, 5]) and $m = 4$ (quadrisection) have been discussed from the point of view of composite schemes in [31], and that $m = 7$ is the next admissible dilation factor for triangular meshes. The motivation for hex-by-7 schemes is not so much a matter of the theory of subdivision surfaces or an anticipated need for another algorithm for surface modelling but the potential use in other applications, e.g., pyramid algorithms for human vision modeling or terrain description in geophysics, where hexagonal grids have been popular for various reasons. The hex-by-7 refinement offers some directional features which can be built into wavelet spaces associated with the multiscale ladders of subspaces defined by the subdivision operator.

First of all, we choose

$$M = \begin{pmatrix} 2 & 1 \\ -1 & 3 \end{pmatrix}, \qquad \det(M) = 7, \tag{14}$$

to describe the dilation on a uniform type-I triangulation. On a uniform hexagonal grid, this corresponds to a counter-clockwise grid rotation by $\phi = \arctan(\sqrt{3}/5)$, whereas the alternative choice

$$M = \begin{pmatrix} 3 & -1 \\ 1 & 2 \end{pmatrix} \tag{15}$$

corresponds to a clockwise rotation by the same angle, this latter case was shown in Figure 3 c). In order to apply our analysis tools as is, the rotation pattern (i.e., M) has to be the same in all subdivision steps. On general triangulations, this consistency in choosing the refinement pattern corresponds to assuming an *orientable triangulation*. More precisely, we assume that any face $f \in \mathcal{F}$ is given by an *ordered* vertex triple $f = (v_1, v_2, v_3)$ or

$$f \; : \quad v_1 \to v_2 \to v_3 \to v_1$$

which is consistent on the set of all faces: If $e = (v, v') = f \cap f'$ is the common edge of two triangles then its endpoints satisfy $v \to v'$ in exactly one of the ordered vertex representations corresponding to f and f'. Obviously, there are triangulations (such as an triangulated Möbius band) which cannot be oriented in the above sense. If the triangulation is orientable, then the $\sqrt{7}$-refinement consistent with the dilation M from (14) consists of inserting 3 new vertices per old triangle f as in Fig. 8 a). Note that the

orientation induces a unique association $v_i' \leftrightarrow (f, v_i, e_i)$ between new vertices and old triangles, vertices, and edges. To see the uniformity of this TR, the location of v_i' is given by barycentric coordinates of $(4/7, 2/7, 1/7)$ with respect to f and the vertex ordering (v_i, v_{i+1}, v_{i+2}), $i = 1, 2, 3$ (here, $v_4 = v_1$, $v_5 = v_2$). A portion of the refined triangulation $\mathcal{T}' = (\mathcal{V}', \mathcal{F}')$ is depicted in Fig. 8 b), it inherits its orientation from $\mathcal{T} = (\mathcal{V}, \mathcal{F})$. On general triangulations, the two possible orientations lead to different mesh connectivity (and thus different $\mathcal{T}$) due to the way the newly inserted vertices are connected accross old edges: We always have a new edge between two vertices associated with the same old edge (the other new edges are between a new vertex and its associated old vertex, and between new vertices if they are associated with the same old vertex and neighboring f).

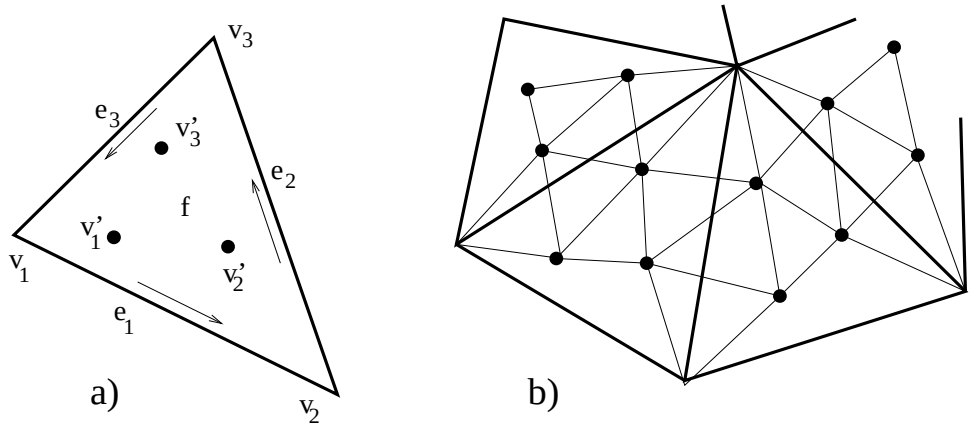


Figure 8: Vertex insertion and $\sqrt{7}$-refinement associated with M given by (14)

Note that in some papers an alternation of the orientation between two consecutive refinement steps has been proposed. This corresponds to alternating the two dilation matrices in (14) and (15), and could still be analyzed by realizing that two consecutive alternating $\sqrt{7}$-refinements are essentially equivalent to a 7-refinement (the same trick was initially applied for $\sqrt{3}$-refinement [3]). However, this leads to $m = 49$ for the new subdivision scheme comprising two alternating $\sqrt{7}$-subdivision steps, with the consequence that the smoothness analysis would require extensive computational efforts.

The next step is the construction of some lower-order schemes with a subdivision operator $S_\mathcal{V}$ of the form (10). The simplest candidate for $\sqrt{7}$-refinement

$$S_1 := (\mathcal{V} \overset{6/7}{\leftarrow} \mathcal{V}) \circ GR_7. \tag{16}$$

is interpolatory, preserves constants, and has minimal stencil support among all schemes with these properties. The position of a new vertex in $\mathbb{R}^3$ is inherited from its associated old vertex. This explains why (16) does not reproduce linear functions and is not useful for geometric applications as is. Note that exactly this S_1 was the prolongation operator of choice in the hex-by-7 pyramid algorithms originally considered in [1] and applied in [37, 26]). Here, we use S_1 for creating the family S_1^L of higher-order concatenated schemes. In particular, for $L = 2$ we arrive at another interpolatory scheme $S_{lin} := S_1^2$

which corresponds to natural linear interpolation: It is given by linearly interpolating the values at the old vertices $\mathcal{V}$ within each old triangle f, and inheriting the values at the new vertices $v' \in f$ from this local interpolant. According to the refinement rules this yields a stencil for new vertices as shown in Figure 9 a).

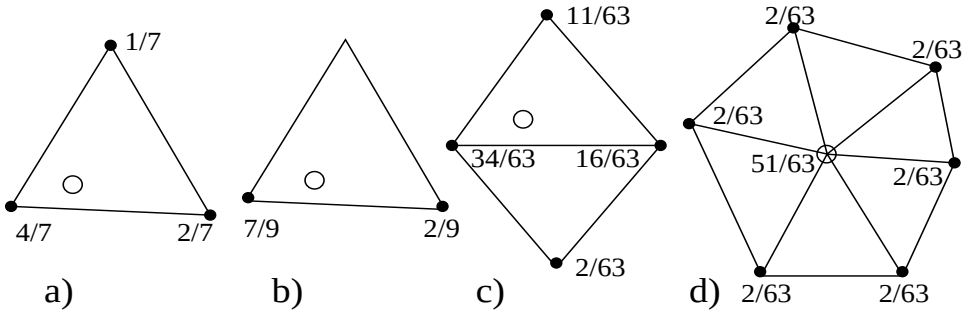


Figure 9: Stencils for new vertex positions for the interpolatory schemes a) $S_{lin} = S_1^2$, b) $S_{\mathcal{V},4/7} = S_2$, and for c) new and d) old vertices for the approximating scheme $S_2 S_1$

Unfortunately, neither S_1 nor $S_{\mathcal{V},lin}$ can be factored in the form (10) such that at least one of the basic averaging rules involves face values. This prevents us from deriving hex-by-seven schemes as a straightforward by-product. As an alternative, we will look for an interpolatory composite scheme of the form

$$S_{\mathcal{V},c} \; : \quad (\mathcal{V}' \leftarrow \mathcal{F}' \overset{c}{\leftarrow} \mathcal{F}' \leftarrow \mathcal{V}') \circ GR_7, \tag{17}$$

and fix the parameter c such that $S_{\mathcal{V},c}$ reproduces at least constants. This is straightforward since the result of $S_{\mathcal{V},c}$ applied to a δ-sequence centered at an arbitrary $v \in \mathcal{V}$ can easily be found, and yields $c = 4/7$. The stencil for new vertices associated with $S_2 := S_{\mathcal{V},4/7}$ is depicted in Fig. 9 b).

While the families of concatenated schemes S_1^L and S_2^L share similar properties (see below), the mask size of the latter will grow faster. To offset this undesirable feature while still being able to switch to a dual scheme with ease, we will also look at the family $S_2 S_1^{L-1}$. The first non-trivial member of this family is $S_2 S_1$, which reproduces linear functions but, in contrast to $S_{lin} = S_1^2$ is not interpolatory anymore, see Fig. 9 c) and d) for the stencils for newly inserted and old vertices in the regular case.

We come to the analysis of the families of concatenated rules S_1^L, S_2^L, and $S_2 S_1^{L-1}$ for values $2 \le L \le 6$ in the regular case. For this, we need the symbols of S_1 and S_2:

$$P_1(\omega) = \frac{1}{7}\left(1 + \sum_{\alpha \in \Lambda_1} e^{-i\alpha\omega}\right), \qquad P_2(\omega) = \frac{1}{7}\left(1 + \left\{\frac{7}{9}\sum_{\alpha \in \Lambda_1} + \frac{2}{9}\sum_{\alpha \in \Lambda_2}\right\} e^{-i\alpha\omega}\right).$$

where the index set Λ_1 corresponds to the vertices in the 1-ring around the origin, while Λ_2 are those indices from the 2-ring that do not belong to $2\Lambda_1$. These symbol functions are real-valued for $\omega \in \mathbb{T}^2$, and possess the symmetries typical for regular triangular meshes (see [10, 9, 12] for how to explore those). Obviously, $P_i(\omega)^L \ge 0$, $\omega \in \mathbb{T}^2$, holds for even L (but not for odd L !) which can be used for the computation of exact Hölder smoothness exponents.

	Family S_1^L		Family S_2^L		Family $S_2 S_1^{L-1}$	
L	s_∞	s_2	s_∞	s_2	s_∞	s_2
2	0.8708	1.6464	1.6046	1.9814	[1.0772, 1.3463]	1.9111
3	[2.0721, 2.4027]	2.7819	[2.3170, 2.9354]	2.9985	[2.2511, 2.7033]	2.9556
4	3.2929	3.8698	3.9629	3.9999	[3.1380, 3.6381]	3.9769
5	[4.1135, 4.6965]	4.9245	[4.0538, 4.9950]	5.0000	[4.1219, 4.8494]	4.9877
6	5.5638	5.9571	5.9959	6.0000	[5.1097, 5.7979]	5.9933

Table 1: Numerically computed Hölder and Sobolev smoothness exponents

In Table 1 below, we have used the methods described in [21] to determine the properties of the above families in the regular case for $2 \leq L \leq 6$. We report our computations of Sobolev and Hölder smoothness exponents. When intervals are shown then they provide upper and lower estimates of the exact Hölder exponent obtained from the ℓ_∞-joint spectral radius formula. Note that the upper interval bound is believed to be much closer to the exact Hölder exponent than the lower one. When the exponents are characterized by a single finite-dimensional eigenvalue problem then its computed value is given. The important output of this exercise is the confirmation of observations made in [31, 21] for similar families $S_\mathcal{V}^L$ associated with TR with dilation factor $m = 3, 4$. E.g., when L is increased then the predictions for Sobolev and Hölder exponents quickly approach the theoretical limit $K = L$ given by their sum rule order. In all cases we have numerically checked that the shifts of the associated refinable functions are stable (this requires to establish the strict positivity of the eigenfunction of the transition operator (13) corresponding to the largest eigenvalue $\lambda = 1$, see [21]). In particular, the schemes S_1^3 and $S_2 S_1^2$ already yield C^2 limits for regular mesh topologies.

How the smoothness problem near extraordinary vertices can be dealt with will be illustrated on the example of the scheme $S = S_1^3$. It is sufficient to investigate the local subdivision map in a sufficently large neighborhood of the origin of a k-vertex rotationally invariant triangulation $\mathcal{T}$. Since the above S results in relatively small stencils, a 2-ring of triangles around the k-vertex will do (the reader can easily check that no vertex location outside this 2-ring can influence the limit surface in the vicinity of the k-vertex). Using the notation introduced in Fig. 10 and by carefully applying the subdivision operator S, we see that the values a', b_i', c_i', d_i' associated with the vertices of this 2-ring in the refined partition $\mathcal{T}'$ are given by the formulae

$$a' = \frac{31}{49}a + \frac{18}{49k}\sum_{j=1}^{k} b_j, \qquad b_i' = \frac{1}{49}(24a + 3b_{i-1} + 12b_i + 9b_{i+1} + b_{j+2}),$$

$$c_i' = \frac{1}{49}(12a + 9b_i + 24b_{i+1} + 3b_{j+2} + c_i), \quad d_i' = \frac{1}{49}(9a + b_{i-1} + 24b_i + 12b_{i+1} + 3c_i),$$

$i = 1, \ldots, k$ (all sequences are extended from this index set to all of $\mathbb{Z}$ by k-periodicity). To study the eigenvalues and eigenvectors of this $3k+1$-dimensional block-circulant local subdivision operator S_0, it is customary to switch within the b, c and d-blocks to the DFT basis of length k, and to reorder the whole matrix correspondingly. This leads to

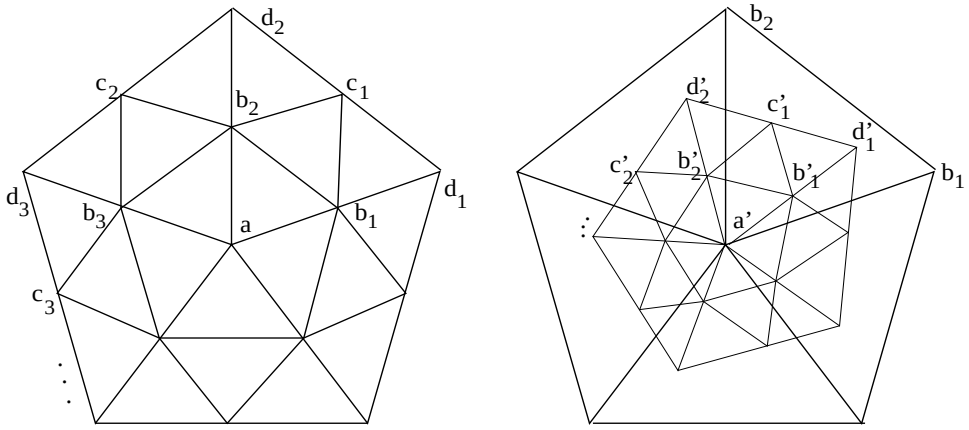


Figure 10: Notation for the local subdivision map

a block-diagonal matrix representation of S_0 with the same eigenvalues. The diagonal blocks consist of a 4×4 matrix

$$B_0 = \frac{1}{49} \begin{pmatrix} 31 & 18 & 0 & 0 \\ 24 & 25 & 0 & 0 \\ 12 & 36 & 1 & 0 \\ 9 & 37 & 3 & 0 \end{pmatrix},$$

which corresponds to the equation for a' and the 3 transformed equations associated with the DFT vector $(1, \ldots, 1)^T$, and 3×3 matrices $B_j = B(e^{i2\pi j/k})$, $j = 1, \ldots, k-1$, associated with the other $k-1$ DFT vectors of length k, where

$$B(z) = \frac{1}{49} \begin{pmatrix} 3z^{-1} + 12 + 9z + z^2 & 0 & 0 \\ 9 + 24z + 3z^2 & 1 & 0 \\ z^{-1} + 24 + 12z & 3 & 0 \end{pmatrix},$$

is the (partial) symbol for the above block-circulant matrix. The set of eigenvalues of B_0 is $\{1,\ 1/7,\ 1/49,\ 0\}$ while the maximum (in absolute value) of all eigenvalues from the remaining B_j is attained in the blocks B_1 and B_{k-1}. This follows from the fact that

$$\rho(t) := |\lambda_1(B(z))| = \frac{1}{49}|3z^{-1} + 12 + 9z + z^2| = \frac{1}{49}\sqrt{157 + 288\xi + 156\xi^2 + 24\xi^3},$$

where $z = e^{it}$, $\xi = \cos(t)$, is an even, 2π-periodic function of t which strictly decreases on $[0, \pi]$, and that the remaining eigenvalues of $B(z)$ are $\lambda_2(B(z)) = 1/49 = \rho(\pi) \leq \rho(t)$, and $\lambda_3(B(z)) = 0$ are smaller. It turns out that $\rho(2\pi/3) = 1/7$, and we conclude that for $k > 4$ there is a pair $\{\lambda_2, \lambda_3\}$ of subdominant eigenvalues $1 = \lambda_1 > |\lambda_2| = |\lambda_3| > |\lambda_4| \geq \ldots$ which are conjugate to each other and belong to B_1 resp. B_{k-1}. This is the standard situation in which the C^1 property typically holds (see [32]). For $k = 3$ this is no longer true since we have a triple $|\lambda_2| = |\lambda_3| = \lambda_4 = 1/7$ of subdominant eigenvalues, the additional one coming from the block B_0.

Since a mathematically rigorous treatment would require the study of the characteristic map [32, 30, 40] and become very technical, we retreat to a visual inspection. In

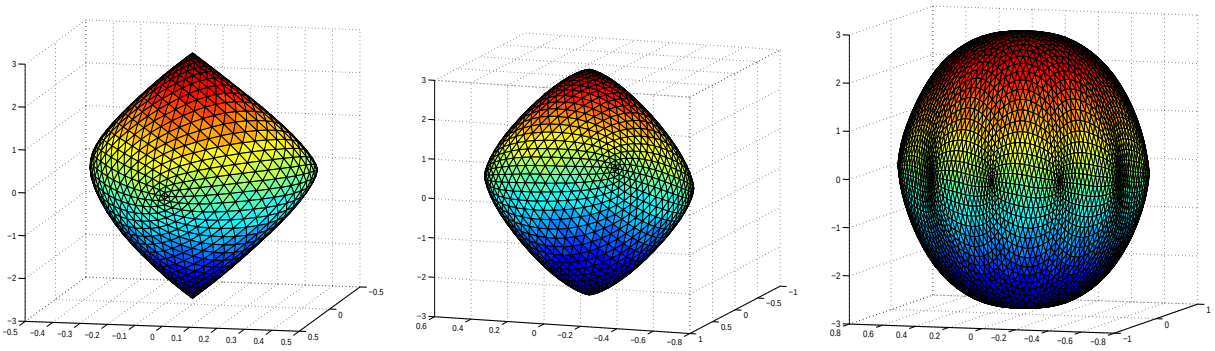


Figure 11: Result after 3 subdivision steps with $S = S_1^3$ applied to a double pyramid over a regular k-gon for $k = 3$ (left), $k = 4$ (center), and $k = 12$ (right)

Figure 11, we show the result of $J = 3$ subdivision steps with the operator S applied to a (symmetric) double pyramid over a regular k-gon as initial configuration. Thus, $\mathcal{T}^0$ contains $2k$ triangular faces, two vertices of valence k, and k vertices (along the base) of valence 4. The pictures clearly support the above findings.

Obviously, for $k = 3$ we need to fix the C^1 property but there is also some desire to generally improve the shape of the resulting surfaces for $k \neq 6$ (e.g., the surface becomes very flat near the tip of the original pyramid for $k = 12$). Within the context of composite schemes, this can most elegantly be done by modifying one or several of the AR involved. This idea was first proposed in [31]. For $S = S_1^3$, we can simply replace the last S_1 by $\mathcal{V} \overset{c}{\leftarrow} \mathcal{V}$, and try to adjust the value $c = c_k$ depending on the valence k. If this modification is applied then this modifies only the value a' at the origin of the k-vertex rotationally invariant neighborhood (all other vertices in this triangulation are regular). The new equation is

$$a' = \frac{49 - 21c}{49} a + \frac{21c}{49k} \sum_{j=1}^{k} b_j,$$

which has no impact on the definition of $B(z)$ and thus on the eigenvalues of the B_j, $j = 1, \ldots, k-1$. However, the first row of B_0 is altered, and the parameter c can be used to change the subdominant eigenvalue $\lambda' = (25 - 21c)/49$ of B_0. E.g., setting

$$c = c_k := \frac{1}{21}(25 - \frac{1}{49}(157 + 288\xi_k + 156\xi_k^2 + 24\xi_k^3)), \qquad \xi_k = \cos(2\pi/k), \tag{18}$$

implies $\lambda' = |\lambda_2|^2 = |\lambda_3|^2$ which is a desirable property (see [29] for some motivation). Any $c_3 \in (6/7, 32/21)$ would formally lead to a pair (instead of a triple) of subdominant, complex-conjugate eigenvalues associated with B_1 and B_2 which is prerequisite for establishing the C^1 property for extraordinary vertices of valence $k = 3$. In Figure 12, we show the same double pyramid examples as in Fig. 11, now with the modified composite scheme $(\mathcal{V} \overset{c_k}{\leftarrow} \mathcal{V}) \circ S_1^2$ using formula (18). Note the considerable improvement for $k = 3, 4$ but also a less flat appearance near the pyramid tip for $k = 12$.

We caution the reader that these considerations are by no means precise mathematical statements, however, they serve as a preliminary assessment of the modified scheme

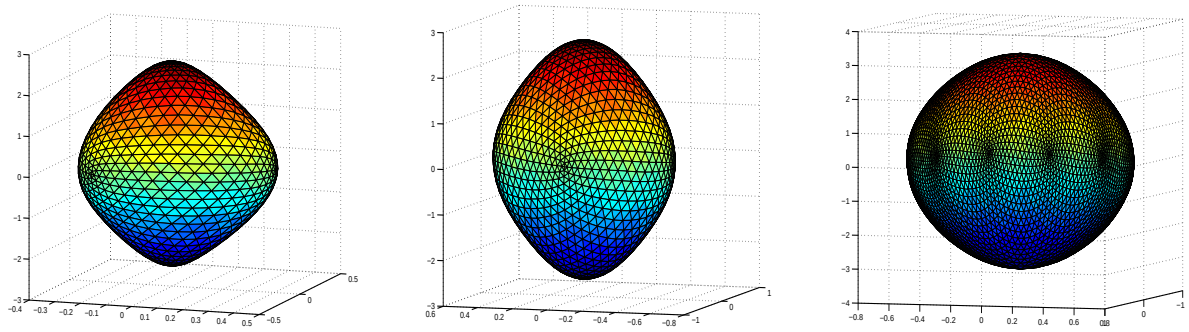


Figure 12: Modification of S_1^3 using (18), applied to the examples of Fig. 11

S_1^3. Similar results can be obtained for $S_2 S_1^2$ if the flap modification in Figure 7 with suitable weight $w = w_k$ replaces the $\mathcal{V} \leftarrow \mathcal{F}$ rule in S_2. Obviously, this scheme can also be rearranged into a hex-by-7 scheme with similar properties.

References

[1] E. H. Adelsson, E. Simoncelli, and R. Hingorani, Orthogonal pyramid transforms for image coding, Proc. SPIE Vis. Commun. Image Process., v. 845, 1987, 50–58.

[2] L. Barthe, L. Kobbelt, Subdivision scheme tuning around extraordinary vertices, Preprint RWTH Aachen, July 2003.

[3] M. Botsch, S. Steinberg, S. Bischoff, L. Kobbelt, OpenMesh - a generic and efficient mesh data structure, Preprint, RWTH Aachen, 2003.

[4] A. S. Cavaretta, W. Dahmen, C. A. Micchelli, Stationary subdivision, Memoirs AMS, vol. 93, AMS, Providence, 1991.

[5] J. Claes, K. Beets and F. van Reeth, A corner-cutting scheme for hexagonal subdivision surfaces, Proc. Int. Conf. "Shape Modeling and Applications", Canada, 2002.

[6] N. Dyn, D. Levin, Subdivision schemes in geometric modelling, Acta Numerica 11 (2002), 73–144.

[7] N. A. Dodgson, I. P. Ivrissimtzis, and M. A. Sabin, Characteristics of dual triangular $\sqrt{3}$ subdivision, in Curve and Surface Fitting: Saint Malo 2002, A. Cohen, J.-L. Merrien, L. L. Schumaker (eds.), Nashboro Press, Brentwood, 2003, pp. 119–128.

[8] N. Dyn, D. Levin, J. Simoens, Face value subdivision schemes on triangulations by repeated averaging, in Curve and Surface Fitting: Saint Malo 2002, A. Cohen, J.-L. Merrien, L. L. Schumaker (eds.), Nashboro Press, Brentwood, 2003, pp. 129–138.

[9] B. Han, Computing the smoothness exponent of a symmetric multivariate refinable function, SIAM J. Matr. Anal. Appl., Vol. 24, No. 3 (2003), 693–714.

[10] B. Han, Classification and construction of bivariate subdivision schemes, in Curve and Surface Fitting: Saint Malo 2002, A. Cohen, J.-L. Merrien, L. L. Schumaker (eds.), Nashboro Press, Brentwood, 2003, pp. 187–198.

[11] B. Han, R.-Q. Jia, Multivariate refinement equations and convergence of subdivision schemes, SIAM J. Math. Anal., Vol. 29, No. 5 (1998), 1177–1199.

[12] B. Han, M. L. Overton, and T. P.-Y. Yu, Design of Hermite subdivision schemes aided by spectral radius optimization, SIAM J. Sci. Comp., (2003, to appear).

[13] I. P. Ivrissimtzis, N. A. Dodgson, and M. A. Sabin, A generative classification of mesh refinement rules with lattice transformations, Preprint, Cambridge Univ. 2002.

[14] I. P. Ivrissimtzis, H.-P. Seidel, Evolutions of polygons in the study of subdivision surfaces, Preprint, MPI Informatik Saarbrücken, Nov. 2003.

[15] I. P. Ivrissimtzis, K. Shrivastava, H.-P. Seidel, Subdivision rules for general meshes, in Curve and Surface Fitting: Saint Malo 2002 A. Cohen, J.-L. Merrien, L. L. Schumaker (eds.), Nashboro Press, Brentwood, 2003, pp. 229–237.

[16] H. Ji, S. D. Riemenschneider, Z. Shen, Multivariate compactly supported fundamental refinable functions, duals, and biorthogonal wavelets, Stud. Appl. Math. 102 (1999), 173–204.

[17] R. Q. Jia, Characterization of smoothness of multivariate refinable functions in Sobolev spaces, Trans. Amer. Math. Soc. 351 (1999), 4089–4112.

[18] R. Q. Jia, Q. Jiang, Spectral analysis of the transition operator and its applications to smoothness analysis of wavelets, SIAM J. Matrix Anal. Appl., to appear.

[19] Q.-R. Jia, S. Zhang, Spectral properties of the transition operator associated to a multivariate refeinement equation, Linear Algebra and its Applications, 292 (1999), 155–178.

[20] Q. Jiang, Multivariate matrix refinable functions with arbitrary matrix dilation, Trans. Amer. Math. Soc. 351 (1999), 2407–2438.

[21] Q. Jiang and P. Oswald, Triangular $\sqrt{3}-$subdivision schemes: The regular case, JCAM 156 (2003), 47–75.

[22] L. Kobbelt, $\sqrt{3}$ subdivision, Proc. SIGGRAPH 2000, 103–112.

[23] M. Kohler, A Meta Scheme for Iterative Refinement of Meshes, Preprint, Uni Dortmund, 1998.

[24] A. Levin, D. Levin, Analysis of quasi-uniform subdivision, ACHA, 15 (2003), 18–32.

[25] C. Loop, Smooth subdivision based on triangular meshes, Master's Thesis, Univ. Utah, Dep. of Mathematics, 1987.

[26] A. Lundmark, N. Wadströmer, H. Li, Hierarchical subsampling giving fractal regions, IEEE Trans. on Image Proc., vol. 10, no. 1, Jan. 2001, 167– 173.

[27] H. Müller, M. Rips, Another Metascheme of Subdivision Surfaces, Research Report no. 713, Uni Dortmund, June 1999.

[28] J. Peters, U. Reif, Analysis of algorithms generalizing B-spline subdivision, SIAM J. Numer. Anal. 35, 2 (1998), 728–748.

[29] J. Peters, U. Reif, Shape Characterization of Subdivision Surfaces – Basic Principles, Preprint 2003.

[30] H. Prautzsch, U. Reif, Necessary conditions for subdivision surfaces, Adv. in Comput. Math. 10 (1999), 209–217.

[31] P. Oswald, P. Schroeder, Composite primal/dual $\sqrt{3}-$subdivision schemes, CAGD 20, 3 (2003), 135–164.

[32] U. Reif, A unified approach to subdivision algorithms near extraordinary points, CAGD 12 (1995), 153–174.

[33] A. Ron, Z. Shen, K. C. Toh, Computing the Sobolev regularity of refinable functions by Arnoldi method, SIAM J. Matrix Anal. Appl., 23 (2001), 57–76.

[34] M. Sabin, in Curve and Surface Fitting: Saint Malo 2002 A. Cohen, J.-L. Merrien, L. L. Schumaker (eds.), Nashboro Press, Brentwood, 2003,.

[35] K. Sahr, D. White, Discrete global grid system, Proc. 30th Symposium on the Interface Computing Science and Statistics 30, 1998, 269–278.

[36] L. Velho, Stellar subdivision grammars, Eurographics (2003).

[37] A. B. Watson, A. J. Ahumada, Jr., A hexagonal orthogonal-oriented pyramid as a model of image presentation in visual cortex, IEEE Trans. Biomed. Eng. vol. 36, no. 1, Jan. 1989, 97–106.

[38] X. Wu, D. Thompson, R. Machiraju, A generalized corner-cutting subdivision scheme, manuscript, 2002.

[39] D. Zorin, A method for analysis of C^1-continuity of subdivision surfaces, SIAM J. Numer. Anal. 37, 5 (2000), 1677-1708.

[40] D. Zorin, Smoothness of stationary subdivision on irregular meshes, Constr. Approx. 16 (2000), 359–397.